Taylor & Francis
Taylor & Francis Group

Philosophical Magazine

ISSN: 1478-6435 (Print) 1478-6443 (Online) Journal homepage: http://www.tandfonline.com/loi/tphm20

A phase-field study of the aluminizing of nickel

T. Philippe, D. Erdeniz, D.C. Dunand & P.W. Voorhees

To cite this article: T. Philippe, D. Erdeniz, D.C. Dunand & P.W. Voorhees (2015) A phase-field study of the aluminizing of nickel, Philosophical Magazine, 95:9, 935-947, DOI: 10.1080/14786435.2015.1010622

To link to this article: http://dx.doi.org/10.1080/14786435.2015.1010622

Philosophical Magazine, 2015
Vol. 95, No. 9, 935–947, http://dx.doi.org/10.1080/14786435.2015.1010622

A phase-field study of the aluminizing of nickel

T. Philippe[a,b]*, D. Erdeniz[a], D.C. Dunand[a] and P.W. Voorhees[a]

[a]*Department of Materials Science and Engineering, Northwestern University, Evanston, IL 60208, USA;* [b]*Normandie Université, Groupe de Physique des Matériaux (GPM), UMR CNRS 6634 BP 12, Avenue de l'Université, 76801 Saint Etienne du Rouvray, France*

(*Received 17 December 2013; accepted 16 January 2015*)

A quantitative phase-field approach for multiphase systems that is based upon CALPHAD free energies is used to model the aluminization of nickel wires, wherein vapour-phase alloying is used to deposit Al on the surface of the Ni wire and then the wire is annealed so that to remove all Al gradients and achieve a homogenous Ni-Al alloy. Both processes are modelled and numerical results are compared with experiments. It is found that the kinetics of both processes is controlled by bulk diffusion. During aluminization at 1273 K, formation and growth of intermetallics, Ni_2Al_3 NiAl and Ni_3Al, are strongly dependent on the Al content in the vapour phase. Ni_2Al_3 growth is very fast compared with NiAl and Ni_3Al. It is also found that an intermediate Al content in the vapour phase is preferable for aluminization, since the Ni_2Al_3 coating thickness is difficult to control. Ni_2Al_3 is found to disappear in a few minutes during homogenization at 1373 K. Thereafter, the NiAl phase, in which the composition is highly non-uniform after aluminization, continues growing until the supersaturation in this phase vanishes. Then, NiAl coating disappears concomitantly with the growth of Ni_3Al, which disappears thereafter. Finally, the Al concentration profile in Ni(Al) homogenizes.

Keywords: Phase-field method; coatings; diffusion; phase transformations

1. Introduction

Aluminization by pack-cementation of nickel-based macroscopic objects such as turbine blades has been used for decades to create near-equiatomic NiAl or Ni_2Al_3 coatings that are oxidation and corrosion resistant [1–3]. Recently, aluminization of sub-millimetre nickel wires [4], struts in nickel foams [5,6] or LIGA nickel objects [7] was performed as a means to alloy the wire in its entirety, whereby the coating is then diffused into the bulk to achieve a gradient-free composition. During the vapour-phase aluminization process, Al is supplied to the Ni surface through the vapour phase in the form of halide that decomposes on the surface and forms shells of one or more intermetallic compounds such as Ni_3Al, NiAl and Ni_2Al_3 [8–11], which grow and shrink upon subsequent interdiffusion.

Multiphase diffusion problems are generally investigated solving Fick's equations for mass transport where the motion of the interfaces between phases is dependent on the difference between the diffusional fluxes [11–13]. The main difficulty for modelling

*Corresponding author. Email: thomas.philippe@univ-rouen.fr

the aluminization of Ni layers is the significant composition-dependence of the interdiffusion coefficient in the non-stoichiometric NiAl phase, which has been shown to vary by more than two orders of magnitude with changes in Ni/Al ratio [13–16]. Interdiffusivities are almost constant in the other compounds and are often considered as concentration-independent in the numerical approaches [13,17,18]. Only a few studies deal with the composition-dependence of the diffusion coefficients and account for all the phases involved in the aluminization and homogenization processes. This composition-dependence can be easily implemented in the phase-field method [19–22] that, in addition, naturally accounts for the Gibbs–Thomson effect that modifies the interfacial compositions, and therefore the diffusion fluxes, for non-planar interfaces.

Multiphase diffusion models for the aluminization of Ni have been developed under conditions of constant surface Al concentration [4,10,17,18] and for the sake of simplicity, the Ni_3Al and NiAl phases are often neglected in the simulation of the high-pack aluminization process [4]. The intermetallic compounds are commonly assumed to nucleate quickly so that the kinetics of the process is controlled by the competitive growth of each phase. Here, we propose to use a phase-field approach to simulate each step of the aluminization process where the driving forces are the chemical potentials that follow from CALPHAD free energies. Composition-dependent interdiffusion coefficients employed in the phase-field method are taken from literature [13–17]. The advantage of this phase-field approach is that it accounts for both kinetics and thermodynamics of the aluminization process, and thus will yield a predictive description of the overall process. In the present study, all the phases involved in the aluminization of Ni are taken into account and the composition dependence of the interdiffusion coefficient in the NiAl phase has also been included.

We use a quantitative phase-field model for multiphase system recently developed by Moelans that can accurately reproduce bulk diffusion controlled growth or interface-limited kinetics [19–22]. After a concise description of the phase-field approach, the method is used to predict microstructure evolution during vapour-phase Al-alloying of Ni wires and subsequent annealing of the aluminized Ni wires. Numerical results are compared to experiments and used to optimize the aluminization process.

2. Phase-field model

Let us consider a system of n components ($k = 1, \ldots, n$) and p phases ($\rho = 1, \ldots, p$) at constant pressure, temperature and molar volume. The concentration field is represented by $n-1$ independent components:

$$\vec{c} = \begin{pmatrix} c_1 \\ \vdots \\ c_{n-1} \end{pmatrix} \tag{1}$$

and the p phases are represented by non-conserved orders parameters:

$$\vec{\eta} = \begin{pmatrix} \eta_1 \\ \vdots \\ \eta_p \end{pmatrix} \tag{2}$$

such as in the ρ phase, $\eta_\rho = 1$ and $\eta_\sigma = 0$ for $\sigma \neq \rho$ and across an interface the order parameters vary smoothly and monotonously.

The free energy of the system is expressed by:

$$F = \int_V \left\{ \sum_\rho \phi_\rho f_\rho(\vec{c}_\rho) + m f_0(\vec{\eta}) + \frac{\kappa(\vec{\eta})}{2} \sum_\rho (\nabla \eta_\rho)^2 \right\} dV \tag{3}$$

where the φ_ρ are the interpolation functions proposed by Moelans [19–22]:

$$\phi_\rho = \frac{\eta_\rho^2}{\sum_\rho \eta_\rho^2} \tag{4}$$

which can be interpreted as phase fractions such as $\sum_\rho \phi_\rho = 1$ and have the following properties:

$$\left.\frac{d\phi_\rho}{d\eta_\sigma}\right|_{\eta_\sigma=0} = \left.\frac{d\phi_\rho}{d\eta_\sigma}\right|_{\eta_\sigma=1,\eta_{\rho\neq\sigma}=0} = 0 \tag{5}$$

f_ρ is the free energy density of the ρ phase (in J/m^3). The virtual compositions $\vec{c}_\rho$ are given by conditions that the diffusion chemical potentials $\tilde{\mu}_k$ are equal at each position for each component:

$$\tilde{\mu}_{\rho,k} = \tilde{\mu}_k = \frac{\partial f_\rho(\vec{c}_\rho)}{\partial c_{\rho,k}} \quad \forall \rho,\ \forall k \tag{6}$$

and are related by mass conservation:

$$\vec{c} = \sum_\rho \phi_\rho \vec{c}_\rho \tag{7}$$

In ρ phase, $\vec{c} = \vec{c}_\rho$ and $\sum_\rho \phi_\rho f_\rho(\vec{c}_\rho) = f_\rho(\vec{c})$. They are called virtual compositions, since this holds at all positions in the system, including the interfacial region. f_0 is a 4th-order Landau polynomial:

$$f_0 = \sum_\rho \left(\frac{\eta_\rho^4}{4} - \frac{\eta_\rho^2}{2} \right) + \sum_\rho \sum_{\sigma\neq\rho} \frac{\gamma_{\rho,\sigma}}{2} \eta_\rho^2 \eta_\sigma^2 + \frac{1}{4} \tag{8}$$

which has minima for $(\eta_1, \ldots, \eta_\rho, \ldots, \eta_p) = (0, \ldots, 1, \ldots, 0)$. The parameter $\gamma_{\rho,\sigma}$ controls the equilibrium profile of the order parameters at the interface ρ,σ [20] and m is a model parameter.

The gradient energy coefficient is given by [22]:

$$\kappa(\vec{\eta}) = \frac{\sum_\rho \sum_{\sigma\neq\rho} \kappa_{\rho,\sigma} \eta_\rho^2 \eta_\sigma^2}{\sum_\rho \sum_{\sigma\neq\rho} \eta_\rho^2 \eta_\sigma^2} \tag{9}$$

such as $\kappa = \kappa_{\sigma,\rho}$ at the interface σ,ρ.

Time evolution of the concentration field is controlled by an Onsager-type diffusion equation, modified at the interface as proposed by Kim [23]:

$$\frac{\partial c_k}{\partial t} = -\nabla \cdot \vec{J}_k = \nabla \cdot \sum_{i=1}^{n-1} \left\{ M_{ki}(\vec{\eta}, \vec{c}) \nabla \frac{\delta F}{\delta c_i} \right\} \tag{10}$$

Assuming that the mobilities follow a mixture rule:

$$M_{ki}(\vec{\eta}, \vec{c}) = \sum_{\rho} \phi_\rho M_{\rho,ki}(\vec{c}) \tag{11}$$

thus,

$$\frac{\partial c_k}{\partial t} = \nabla \cdot \sum_{i=1}^{n-1} \left\{ \sum_{\rho} \phi_\rho M_{\rho,ki}(\vec{c}) \right\} \nabla \tilde{\mu}_i \tag{12}$$

Classically, the chemical mobility matrix in the ρ phase (M_ρ) can be related to the inter-diffusion coefficients [22]:

$$\tilde{D}_{\rho,ki} = \sum_{j=1}^{n-1} M_{\rho,kj} \frac{\partial^2 f_\rho}{\partial c_j \partial c_i} \tag{13}$$

which is the standard result in multicomponent alloys when the fluxes are written in a volume centred frame.

The evolution of the non-conserved order parameters is assumed to follow:

$$\frac{\partial \eta_\rho}{\partial t} = -L(\vec{\eta}) \frac{\delta F}{\delta \eta_\rho} \tag{14}$$

where the kinetic coefficient is η-dependent:

$$L(\vec{\eta}) = \frac{\sum_\rho \sum_{\sigma \neq \rho} L_{\rho,\sigma} \eta_\rho^2 \eta_\sigma^2}{\sum_\rho \sum_{\sigma \neq \rho} \eta_\rho^2 \eta_\sigma^2} \tag{15}$$

leading to $L(\vec{\eta}) = L_{\rho,\sigma}$ at the interface ρ,σ.

Assuming that $\kappa_{\rho,\sigma} = \kappa$ and $\gamma_{\rho,\sigma} = \gamma$, Equation (14) leads to the following fully variational evolution equation for the order parameters:

$$\begin{aligned} \frac{\partial \eta_\rho}{\partial t} = -L(\vec{\eta}) \Bigg(& m \left[\eta_\rho^3 - \eta_\rho + 2\gamma \eta_\rho \sum_{\sigma \neq \rho} \eta_\sigma^2 \right] - \kappa \nabla^2 \eta_\rho \\ & + \frac{2\eta_\rho}{\sum_\sigma \eta_\sigma^2} \left[(1 - \phi_\rho) \left(f_\rho(\vec{c}_\rho) - \sum_{k=1}^{n-1} \tilde{\mu}_k c_{\rho,k} \right) - \sum_{\sigma \neq \rho} \phi_\rho \left(f_\sigma(\vec{c}_\sigma) - \sum_{k=1}^{n-1} \tilde{\mu}_k c_{\sigma,k} \right) \right] \Bigg) \end{aligned} \tag{16}$$

The parameters m and κ are related to the interface thickness l and to the interfacial energy σ_{int} [20,23–25]. It can be demonstrated [20] that the interfacial energy of an interface between phases ρ, σ is related to m and to the gradient coefficient κ:

$$\sigma_{\text{int}} = g(\gamma) \sqrt{m\kappa} \tag{17}$$

with $g(\gamma) \sim \frac{4}{3} \sqrt{\frac{2\gamma - 1}{4(2\gamma + 1)}}$ a very good approximation (error <2%) of the $g(\gamma)$ function for γ belonging to [0.75,3.45].

By definition, the interface thickness l can also be related to m and κ and a very good approximation for γ belonging to [0.75,3.45] is [20]:

$$l \sim \sqrt{\frac{\kappa}{m}\frac{4(2\gamma+1)}{2\gamma-1}} \tag{18}$$

It was shown that the thin interface limit for infinite interface mobility leads to bulk diffusion controlled growth and following expression of the kinetic coefficient $L_{\rho,\sigma}$ [22]:

$$L_{\rho,\sigma} = \frac{\sqrt{2}mg(\gamma)}{\kappa I(\gamma)\tau_{\rho,\sigma}} \tag{19}$$

with $I(\gamma)$ a γ dependent function (~0.34 for $\gamma = 3$) and $\tau_{\rho,\sigma}$ defined as:

$$\tau_{\rho,\sigma} = \sum_{k=1}^{n-1}\left(c_{\rho,k}^{eq} - c_{\sigma,k}^{eq}\right)\sum_{i=1}^{n-1} m_{ki}\left(c_{\rho,i}^{eq} - c_{\sigma,i}^{eq}\right) \tag{20}$$

The m_{ki} coefficients are the elements of the inverse of the mobilities matrix $\mathbf{M} = M_{ik}$ $M_{ik} = (M_{\rho,ik} + M_{\sigma,ik})/2$. This formulation quantitatively reproduces results in a binary alloy without anti-trapping current, even for a mesoscale interface width [22].

In this study, aluminization of Ni wires was modelled using a mesoscale interface width, 0.4 μm, that is about ten times smaller than the smallest average diffusion-length in the system (~4 μm in the solid solution) so that inaccuracies due to the finite interface width remain negligible [26–32]. We have verified this is indeed the case using analytical solutions for particles of sizes and growth rates seen in the experiments. The axial symmetry of the experiments allows the phase-field equations to be implemented in cylindrical coordinates. Parabolic approximations of the CALPHAD free energy functions were used [33]. Thus Equation (6) with the constraint given by Equation (7) can be solved analytically and therefore it considerably reduces the computation time. When the full CALPHAD representation of the free energies was employed, a suitable root-finding algorithm had to be used to solve this system of non-linear equations [34]. While the parabolic approximation was found to accurately reproduce the thermodynamics of the binary system in the present work, it appears that a more sophisticated description needs to be used to model multicomponent alloys for which the free energy landscapes can exhibit complicated curvatures. The mobility matrices have been directly computed using Equation (13) from the free energy of the phases [33] and the interdiffusion coefficients given in ref. 13, tables II-V. Local equilibrium was assumed at both interfaces so that bulk diffusion controls the motion of the interfaces. The Al surface composition has been chosen to fit the experimental results. This parameter is different for each pack used in the experimental process and depends on the Al activity in the vapour phase. As shown by the experiments, nucleation of the intermetallic phases is very fast at 1273 K. The experimental configuration observed after 5 min of aluminization is used as the initial configuration for the simulations. Coatings are considered as being purely stoichiometric for the initial configuration and their respective thicknesses observed at 5 min are used as input parameters for the simulation.

3. Experimental procedure

Pack aluminization experiments were carried out in a tube furnace under continuous argon flow at 1273 K on Ni (99.95% pure, from MWS Wire Industries) wires with a diameter of 127 μm. For each experiment, five wires, 30–40 mm in length, were

embedded in a powder pack mixture that was contained in an Al_2O_3 crucible. The powder pack mixture consisted of 82 wt.% Al_2O_3 powders (20–50 μm particle size) as the filler, 15 wt.% Al source powders, and 3 wt.% NH_4Cl powders (100 μm particle size) as the activator. Three different types of Al source powders were employed to change the kinetics of the aluminization process. These were pure Al, Ni_2Al_3 (Ni-40 wt.% Al, 150 μm particle size, procured from Goodfellow) and Ni-20 wt.% Al (100–300 μm particle size, arc melted and crushed by ball milling). From here on these packs will be labelled according to their Al compositions, i.e. P100, P40, and P20, respectively. The crucible was closed with a tight Al_2O_3 lid, containing the specimen and the powder mixture. The crucible was pushed into the hot zone of the furnace and held there for various durations (5, 7.5, 10, 15, 30, and 60 min). Time started as soon as the crucible reached the hot-zone of the furnace, which caused a sudden drop of temperature of 45 K. At the end of the process, the crucible was pulled back to the water-cooled end of the furnace.

Select specimens were encapsulated under vacuum in capillary quartz tubes. Encapsulated specimens were homogenized in a box furnace at 1373 K for specified durations (0.25, 0.5, 1, 10, and 24 h). All specimens were mounted in epoxy and prepared for microscopy by means of standard metallographic techniques. An Olympus PMG3 optical microscope and a Hitachi S4800 scanning electron microscope (SEM) equipped with an energy dispersive X-ray spectrometer (EDS) were used for specimen characterization. EDS signal was calibrated by using standard samples of Ni_2Al_3.

4. Results and discussion

The vapour-phase alloying process involves the formation of Ni_2Al_3, NiAl, and Ni_3Al phases. The number of phases involved depends on the Al content in the vapour phase. For instance, a low Al concentration at the surface of the wire may not be sufficient to form a Ni_2Al_3 coating or even a NiAl coating. The purpose of this portion of the paper is to compare the phase-field simulations to the aluminization experiments, so that the code can be used to guide the experiments.

Al concentration profiles in the wire are shown in Figure 1 after 10, 20 and 30 min for a chosen Al surface composition of 55 at.%. Only the Ni(Al), NiAl and Ni_3Al phases are involved in the aluminization process because the Al surface composition is lower than the Al composition in Ni_2Al_3. The unusual shape of the concentration profile in the NiAl phase is due to the very low diffusion coefficient in this phase near its stoichiometry of 50 at.%. The horizontal lines are the compositions of the phases as given by the equilibrium phase diagram. Consistent with the local equilibrium assumption, the compositions of these phases at the interface do not change with time. Figure 1 shows that the width of the Ni_3Al phase region remains constant during aluminization, approximately 1 μm. Thus, most of the growth is in the NiAl phase as the diffusivity in this phase is high in comparison with Ni_3Al and Ni(Al). This scenario is in good agreement with previous studies on the low-pack process [17].

The aluminization process has been investigated experimentally using three different packs: a high Al content pack (denoted P100), a medium Al content pack (P40) and a low Al content pack (P20). As expected these packs gave different coatings. The experimental measurement of the thickness of each phase is an average of five experiments. The high packs involve the formation of NiAl, Ni_3Al or Ni_2Al_3 coatings. Due to the

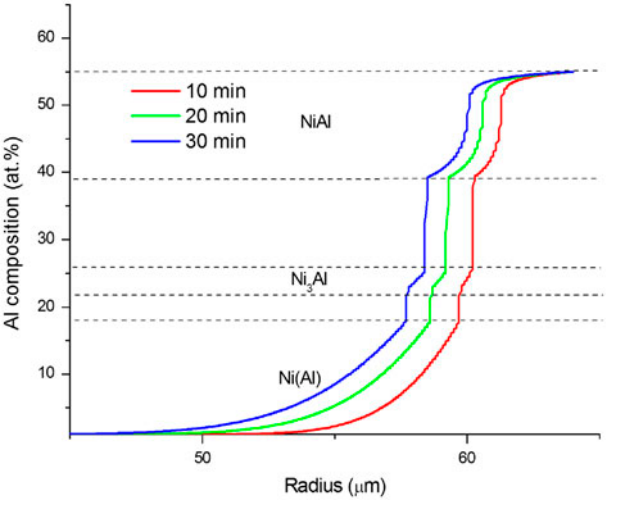

Figure 1. (colour online) Al concentration profiles in a Ni wire for three aluminization times (Al surface composition of 55 at.%) at 1273 K.

very high diffusion coefficient in the Ni_2Al_3 phase, the phase-field simulations show that its growth is very fast and that the Ni_3Al and NiAl coatings remain very thin, which explains why theses phases are almost invisible on the micrographs (not shown here). Moreover, the Ni_2Al_3 coating thickness has been found to be very different from one wire to another and this non-uniformity is the result of the very high diffusivity in this phase (preventing uniform surface diffusion along NiAl). As a result, the microstructure of the high pack case is difficult to control.

The lower Al content in the vapour phase for P40 leads to a thin Ni_2Al_3 coating at the surface of the wire, as shown Figure 2(b) presenting a micrograph of a Ni wire aluminized for 30 min at 1000 °C. NiAl and Ni_3Al are also present (see Figure 2(a) and (b)). The kinetics of the medium pack is much slower than the high pack as the surface Al composition is lower. The coating thicknesses with this pack have been found to be homogeneous from a wire to another. Coating thicknesses have been compared to the numerical predictions in Figure 3. As expected because of its high diffusivity, Ni_2Al_3 was found to grow faster than any other phase. Comparison with the numerical predictions shows a relatively good agreement. The low pack (P20) only entails the formation and growth of Ni_3Al. Ni_3Al thickness as given by the phase-field simulation is given Figure 4 and compared to the experimental results. For both P40 and P20 packs, a reasonable agreement between simulation and experiment was found.

A homogenization step is performed in order to reach the equilibrium state where there are no gradients in Al and Ni across the wire diameter, with the equilibrium state depending on the overall Al composition in the Ni wire, which is dependent on the respective thicknesses of the different coatings. For homogenization, there is no free parameter in the phase-field simulation, contrary to the aluminization case for which the Al content at the surface of the wire was kept constant. As expected because of its high Al content, Ni_2Al_3 coating thickness has a strong influence on the final average Al

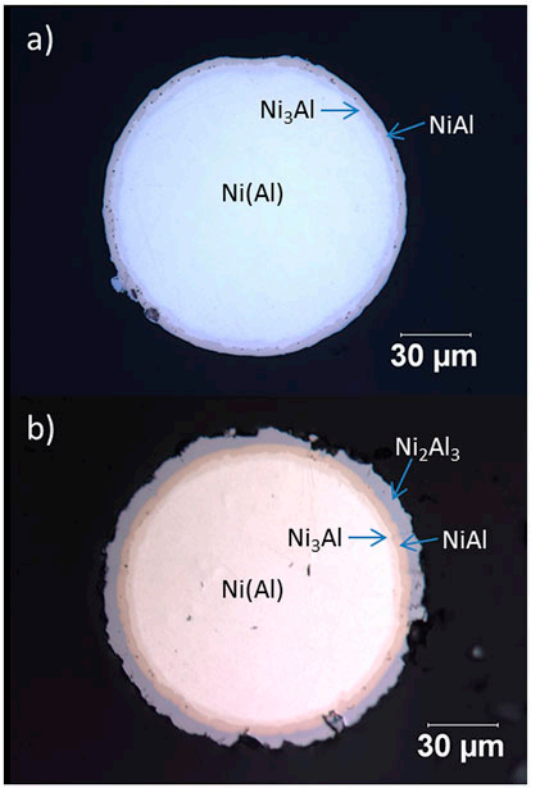

Figure 2. (colour online) Micrographs of Ni wires aluminized at 1273 K for 15 min (a) and 30 min (b).

composition in the Ni wire and a difference of only a few microns in the thickness of this layer leads to a very different equilibrium state. This is illustrated by Figure 5, which shows the predictions of the phase-field simulations for the temporal evolution of the phase thicknesses during homogenization at 1373 K for two different initial Ni_2Al_3 coating thicknesses, i.e. 15 and 18 µm. The equilibrium state is a two-phase system with NiAl on the outside and Ni_3Al on the inside, in agreement with the phase diagram (see Figure 6), as the Al nominal composition in the wire (~0.33 for the 15 µm case and ~0.35 for the 18 µm case) falls in the two-phase (Ni_3Al and NiAl) region. This complicated sequence of phase formation and dissolution, due to changes in the diffusion fluxes at the interfaces, naturally happens with the phase-field method. A difference of a few microns in the initial Ni_2Al_3 coating thickness is shown to lead to very different coating thicknesses. In the 18 µm case, NiAl and Ni_3Al coatings have about the same thickness (~30 µm) whereas the Ni_3Al coating thickness is much larger in the 15 µm case. As previously mentioned, Ni_2Al_3 coating was found to be non-uniform from one wire to another after high pack aluminization, and the previous simulation shows that the high pack is difficult to control.

Coating thicknesses during homogenization at 1373 K of a Ni wire aluminized for 30 min at 1273 K (P40) are compared to the experiments in Figure 7. The initial wire

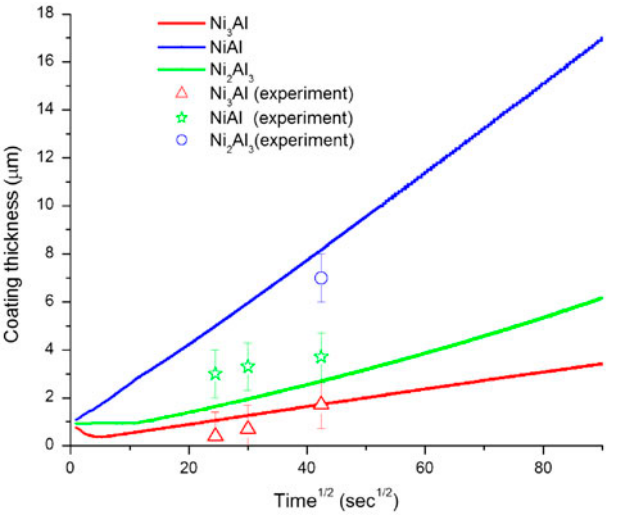

Figure 3. (colour online) Temporal evolution of the thicknesses of three coatings during aluminization (P40 pack). Numerical results are compared to the experiments. Ni_2Al_3 coating at 10 and 15 min is not clearly visible on the micrographs.

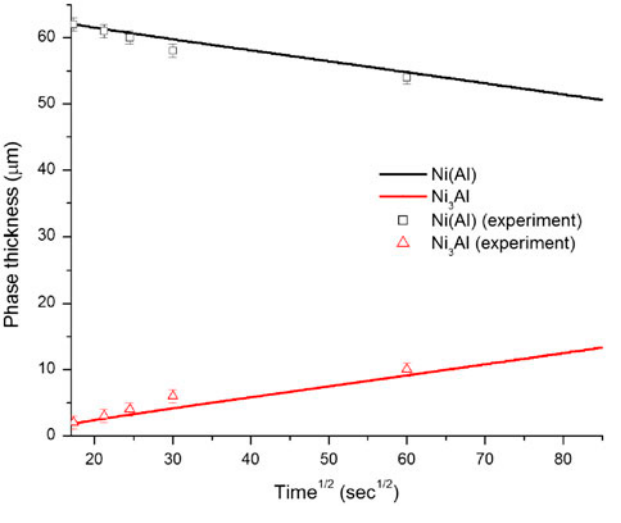

Figure 4. (colour online) Temporal evolution of the Ni(Al) and Ni_3Al phase thicknesses involved in the low pack aluminization process (P20). Numerical results are compared to the experiments.

contains four phases: three coatings (the intermetallic compounds) and the solid solution (not shown in Figure 7). Again, a good agreement was found. As expected, Ni_2Al_3 was found to disappear in a few minutes because of its high diffusivity. Thereafter, the NiAl phase, in which the composition is highly non-uniform, continues growing until the Al

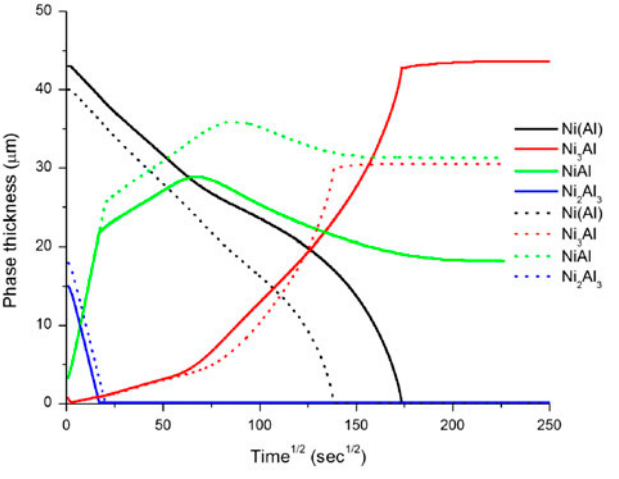

Figure 5. (colour online) Predictions of various phase thicknesses during homogenization (1373 K) for two different initial Ni_2Al_3 thicknesses: 15 μm (solid lines) and 18 μm (dotted lines).

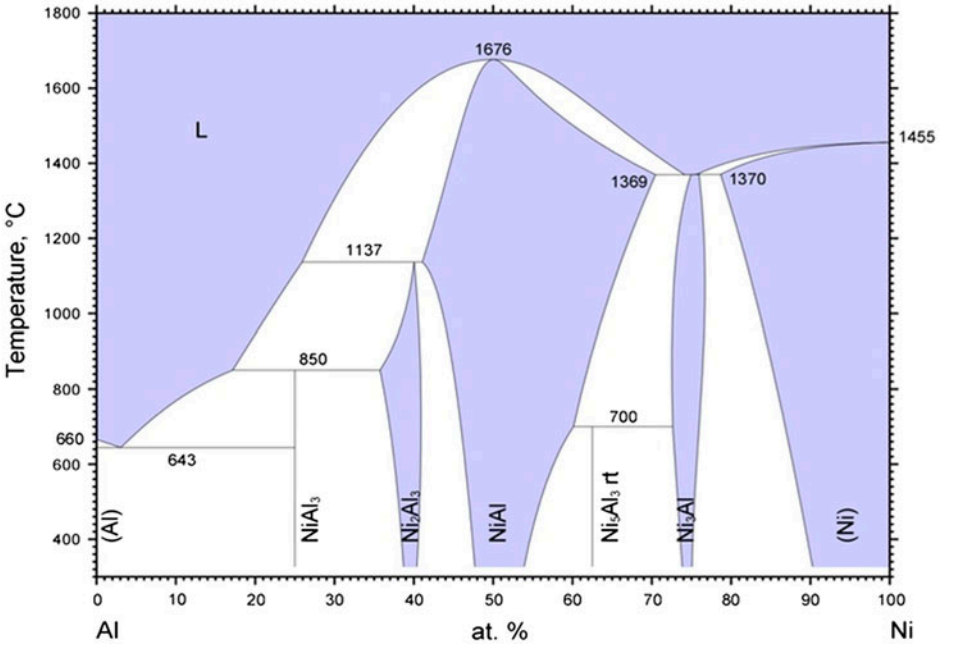

Figure 6. (colour online) Ni-Al phase diagram [35].

concentration gradient in this phase at the NiAl/Ni_3Al interface sufficiently decreases for having Al atoms leave NiAl and enrich the Ni_3Al phase. Then, NiAl disappears concomitantly with the growth of Ni_3Al. The next step corresponds to the

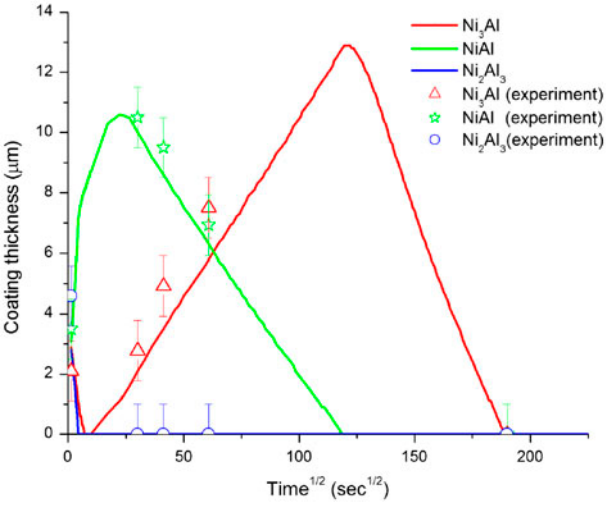

Figure 7. (colour online) Coating thicknesses given by the phase-field simulation during homogenization at 1373 K of the Ni wire aluminized for 30 min (1273 K, medium pack, P40), as compared to the experimental results. The phase-field simulation predicts that ~10 h is required for each coating to disappear. Experiments have confirmed this prediction as no coatings were found after 10 h homogenization ($t^{1/2}$~190 $sec^{1/2}$).

disappearance of Ni_3Al. Finally, the last step requires homogenization of the Al concentration profile in Ni(Al). While the disappearance of Ni_3Al is fast (<10 h), the complete homogenization of the Ni(Al) solid solution requires longer times because of the low diffusivity in this phase near the equiatomic composition. The coating thicknesses evolve approximately as $t^{1/2}$ for both homogenization simulations (Figures 5 and 7). This is consistent with diffusion-limited growth and constant interfacial compositions. Only growth of Ni_3Al and shrinking of NiAl and Ni(Al) behave differently after NiAl reaches ~30 μm for the homogenization simulation presented in Figure 5. This can be explained by a rapid change in the far-field Al composition in the solid solution during shrinking of Ni(Al) as the composition in the centre of the wire rapidly increases during this regime and therefore is expected to lead to non-parabolic thickness evolution. As for aluminization, phase-field simulations can be used to optimize the homogenization process. The good agreement between simulation and experiment for both aluminization and homogenization reveals that bulk diffusion controls the kinetics of both processes as local equilibrium was assumed at the interfaces in the phase-field simulations.

5. Conclusion

A quantitative phase-field approach for multiphase systems was used to model aluminization and homogenization of Ni wires. Numerical results were compared to experiments. It was found that both steps of the aluminization process are controlled by bulk diffusion. During aluminization at 1273 K, formation and growth Ni_2Al_3 NiAl and Ni_3Al phases are strongly dependent on the Al content in the vapour phase. Ni_2Al_3

growth is very fast compared with NiAl and Ni_3Al. It was also found that at an intermediate Al content in the vapour phase is preferable for aluminization since the Ni_2Al_3 coating thickness is difficult to control because of a high interdiffusion coefficient in this phase. Ni_2Al_3 coating is found to disappear in a few minutes during homogenization at 1373 K. Thereafter, the NiAl phase, in which the composition is highly non-uniform, continues growing until the supersaturation in this phase vanishes. Then, NiAl coating disappears concomitantly with the growth of Ni_3Al, which disappears thereafter. The last step corresponds to homogenization of the Al concentration profile in Ni(Al).

Acknowledgements

The authors thank Mr Edward Lee Pang (Northwestern University) for his help with metallography and microscopy and Prof. Kevin Hemker (Johns Hopkins University) for helpful discussions.

Funding

This research was supported by DARPA under contract W91CRB1010004 (Dr Judah Goldwasser, monitor).

References

[1] G.W. Goward and D.H. Boone, Oxid. Met. 3 (1971) p.475.
[2] D.K. Das, V. Singh and S.V. Joshi, Met. Trans. A 29A (1998) p.2173.
[3] G.W. Goward and L.W. Cannon, J. Eng. Gas Turbines Power 110 (1988) p.150.
[4] D.C. Dunand, A.M. Hodge and C. Schuh, Mater. Sci. Technol. 18 (2002) p.326.
[5] H. Choe and D.C. Dunand, Acta Mater. 52 (2004) p.1283.
[6] A.M. Hodge and D.C. Dunand, Intermetallics 9 (2001) p.581.
[7] D.E. Burns, Y. Zhang, M. Teutsch, K. Bade, J. Aktaa and K.J. Hemker, Scripta Mater. 67 (2012) p.459.
[8] L.S. Castleman and L. Seigle, Trans. AIME 212 (1958) p.589.
[9] S.R. Levine and R.M. Caves, J. Electrochem. Soc. 121 (1974) p.1051.
[10] A.J. Hickl and R.W. Heckel, Metall. Trans. A 6 (1975) p.431.
[11] E. Metin, O.T. Inal, A.D. Romig JR, Metall. Mater. Trans. A 36 (2005) 1407.
[12] C. Schuh, Metall. Mater. Trans. A 31 (2000) p.2411.
[13] S. Shankar and L.L. Seigle, Metall. Trans. A 9 (1978) p.1467.
[14] S. Kim and A. Chang, Metall. Mater. Trans. A 31 (2000) p.1519.
[15] T. Helander and J. Ågren, Acta Mater. 47 (1999) p.1141.
[16] H. Wei, X. Sun, Q. Zheng, H. Guan and Z. Hu, Acta Mater. 52 (2004) p.2645.
[17] A.K. Sarkhel and L.L. Seigle, Metall. Trans. A 7 (1976) p.899.
[18] E. Gariboli, M. Verani and C. Riva, Trans. Tech. Publications 278 (2011) p.228.
[19] N. Moelans, B. Blanpain and P. Wollants, Phys. Rev. Lett. 101 (2008) p.025502.
[20] N. Moelans, B. Blanpain and P. Wollants, Phys. Rev. B 78 (2008) p.024113.
[21] N. Moelans, Arch. Metal. Mater. 53 (2008) p.1149.
[22] N. Moelans, Acta Mater. 59 (2011) p.1077.
[23] S.G. Kim, Acta Mater. 55 (2007) p.4391.
[24] S. Kim, W. Kim and T. Suzuki, Phys Rev. E 60 (1999) p.7186.
[25] I. Steinbach, F. Pezzolla, B. Nestler, M. Seeßelberg, R. Prieler and G. Schmitz, Physica D 94 (1996) p.135.
[26] A. Karma and W.J. Rappel, Phys. Rev. Lett. 77 (1996) p.4050.

[27] A. Karma and W.J. Rappel, Phys. Rev. E 53 (1996) p.R3017.
[28] A. Karma and W.J. Rappel, Phys. Rev. E 57 (1998) p.4323.
[29] R.F. Almgren, J. Appl. Math. 59 (1999) p.2086.
[30] A. Karma, Phys. Rev. Lett. 87 (2001) p.115701.
[31] B. Echebarria, R. Folch, A. Karma and M. Plapp, Phys. Rev. E 70 (2004) p.061604.
[32] L. Zhang, E.V. Danilova, I. Steinbach, D. Medvedev, P.K. Galenko, Acta Mater. 61 (2013) p.4155.
[33] N. Saunders, Proc. Int. Symp. Super. (1996) p.101.
[34] J.-L. Fattebert, M.E. Wickett, P.E.A. Turchi, Acta Mater. (2013) Available at http://dx.doi.org/10.1016/j.actamat.2013.09.036.
[35] I. Ansara, N. Dupin, H.L. Lukas and B. Sundman, J. Alloys Compd. 247 (1997) p.20.